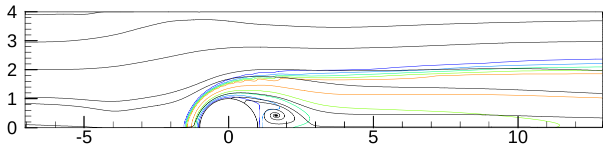

(a) U_{in} = 0.75 m/sec

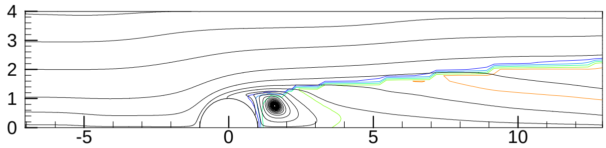

(b) U_{in} = 1.0 m/sec

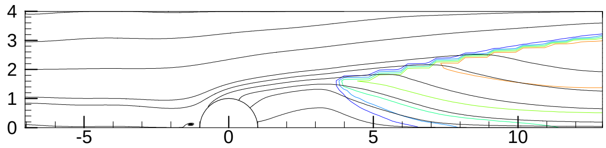

(c) U_{in} = 1.01 m/sec

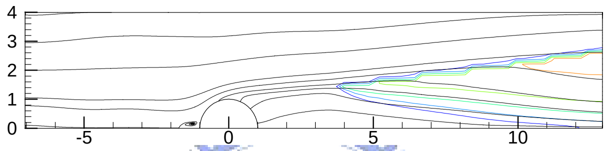

(d) U_{in} = 1.15 m/sec

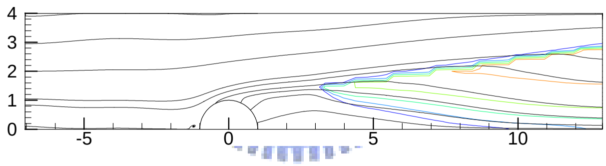

(e) U_{in} = 1.3 m/sec

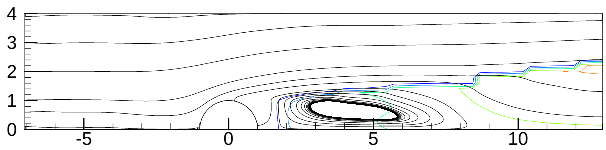

(f) U_{in} = 1.39 m/sec

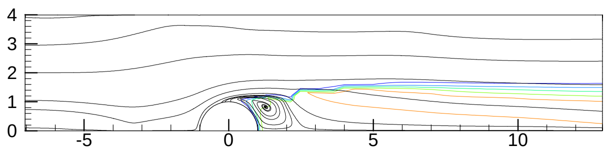

(g) U_{in} = 1.4 m/sec

Fig. 1.1 Series of temperature contour distributions and flow streamlines for a circular cylinder by Tsa (2003)

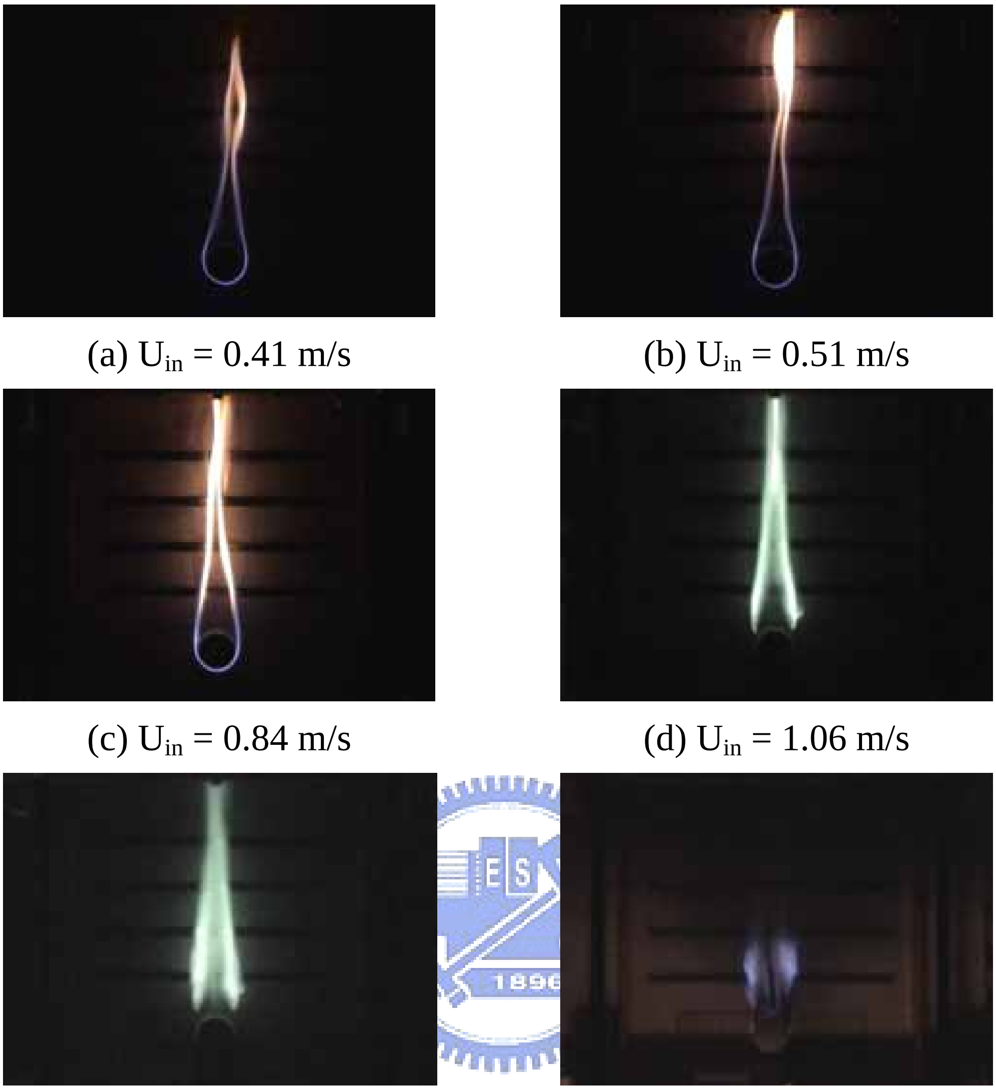

(a) U_{in} = 0.41 m/s
(b) U_{in} = 0.51 m/s
(c) U_{in} = 0.84 m/s
(d) U_{in} = 1.06 m/s
(e) U_{in} = 1.24 m/s
(f) U_{in} =1.63 m/s

Fig. 1.2 Series of flame configurations as a function of incoming flow velocity (V_w = 1.4 cm/s) by Chang (2002)

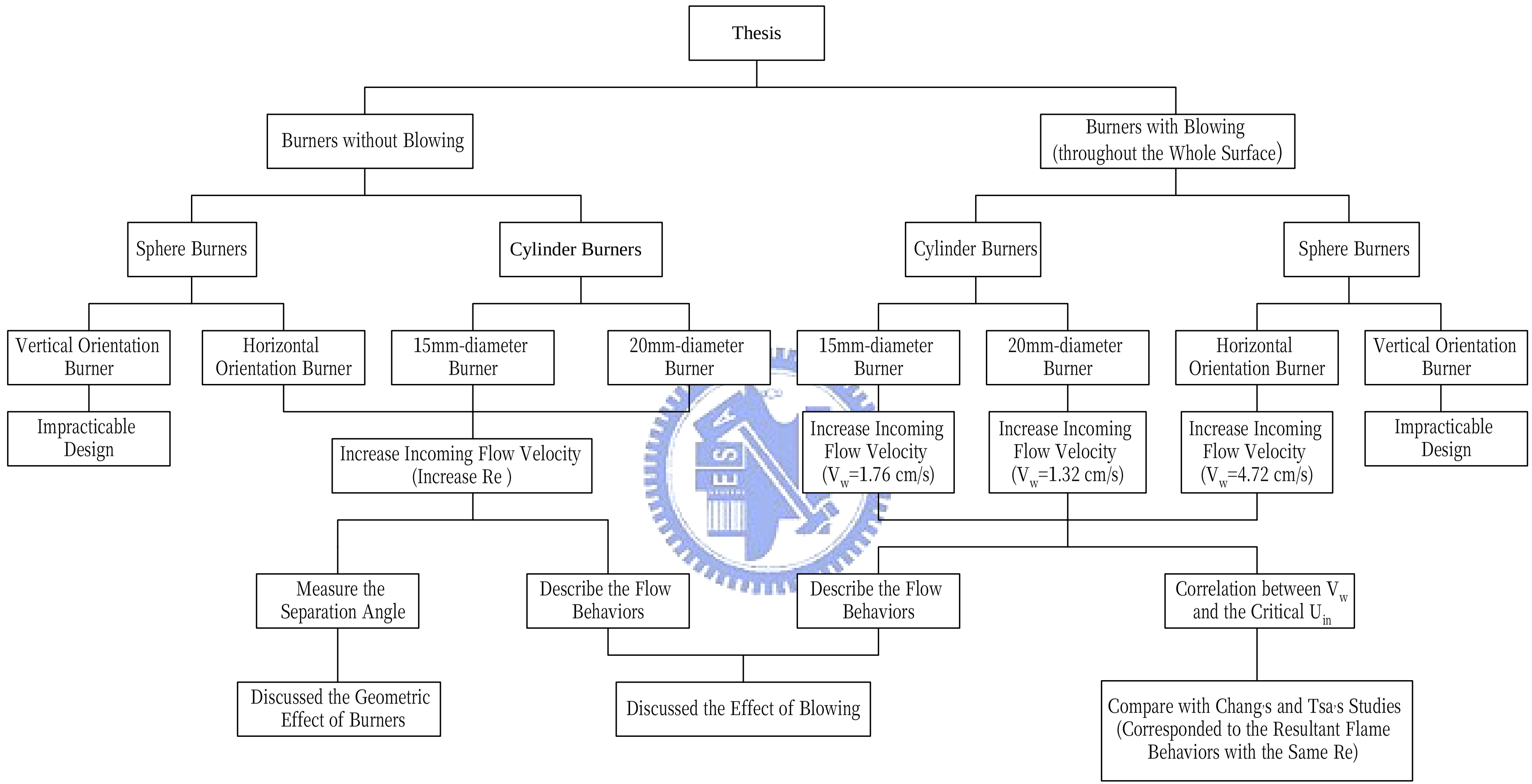

Fig. 1.3 Scheme diagram of the thesis

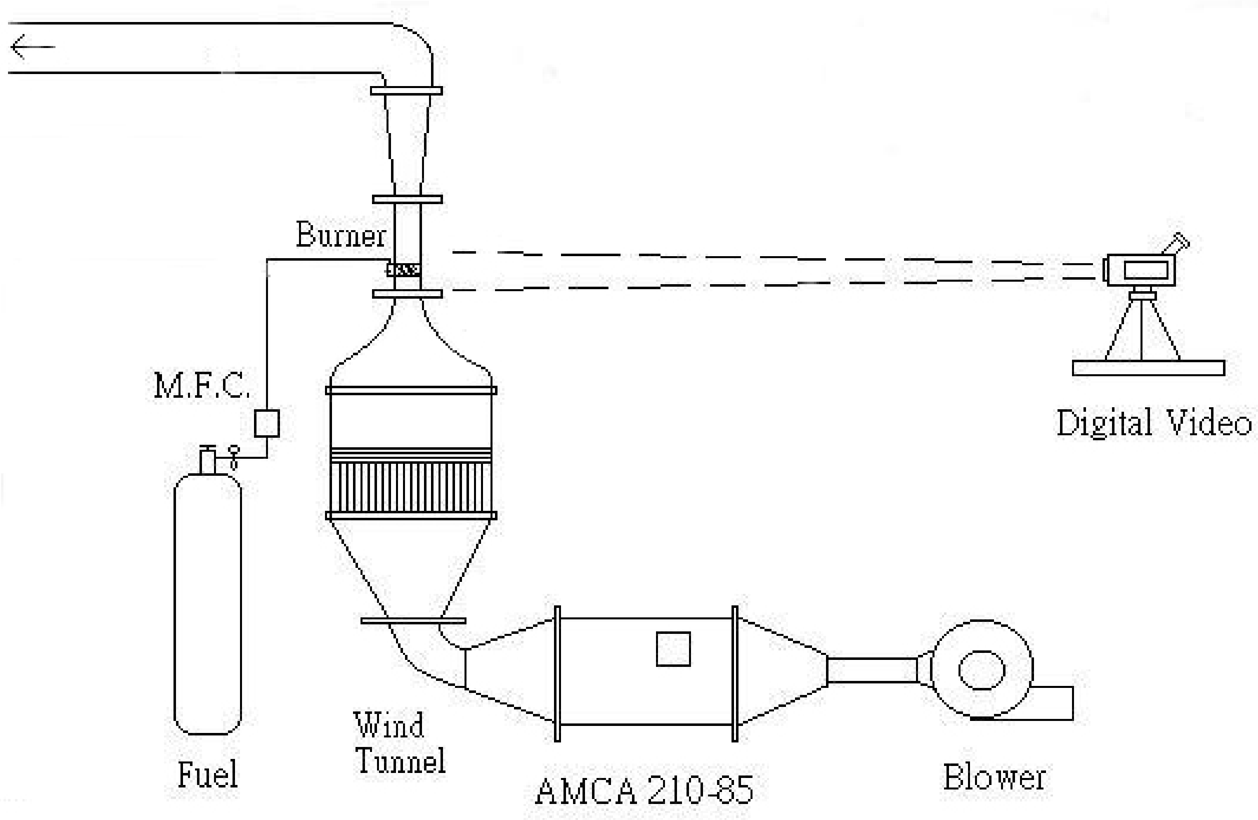

Fig. 2.1 Schematic drawing of overall experimental system

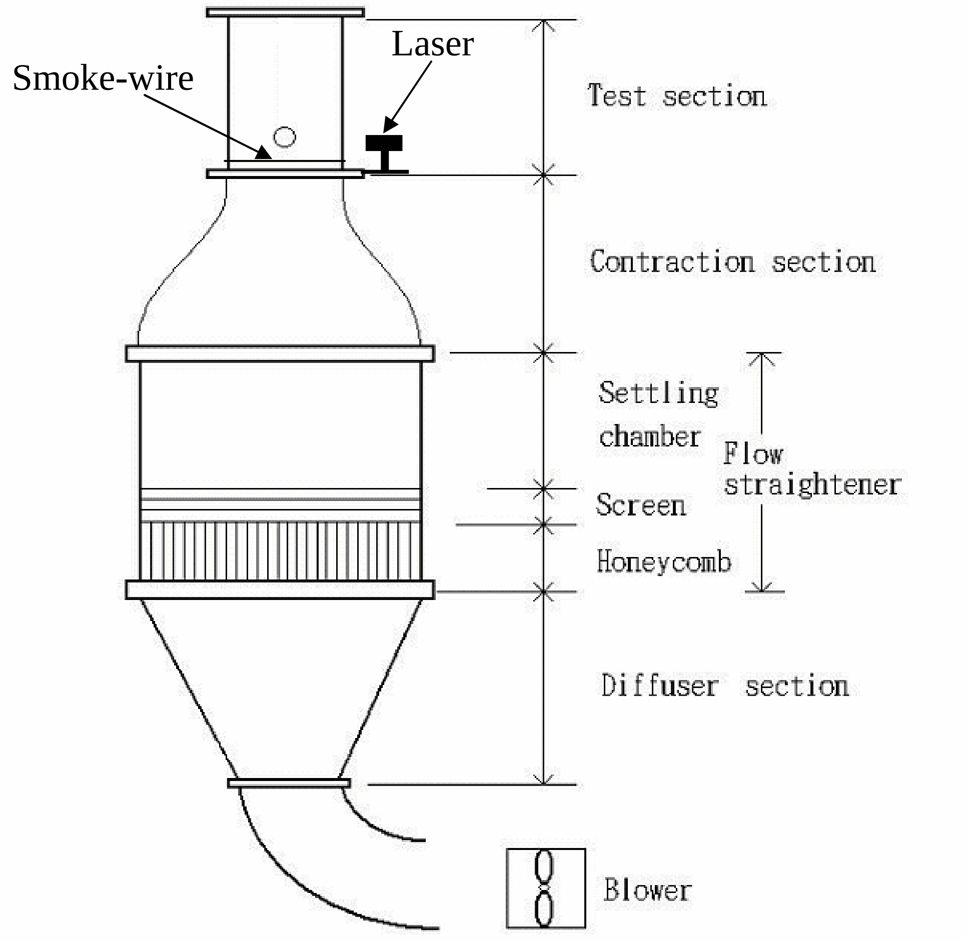

Fig. 2.2 Schema of the wind tunnel

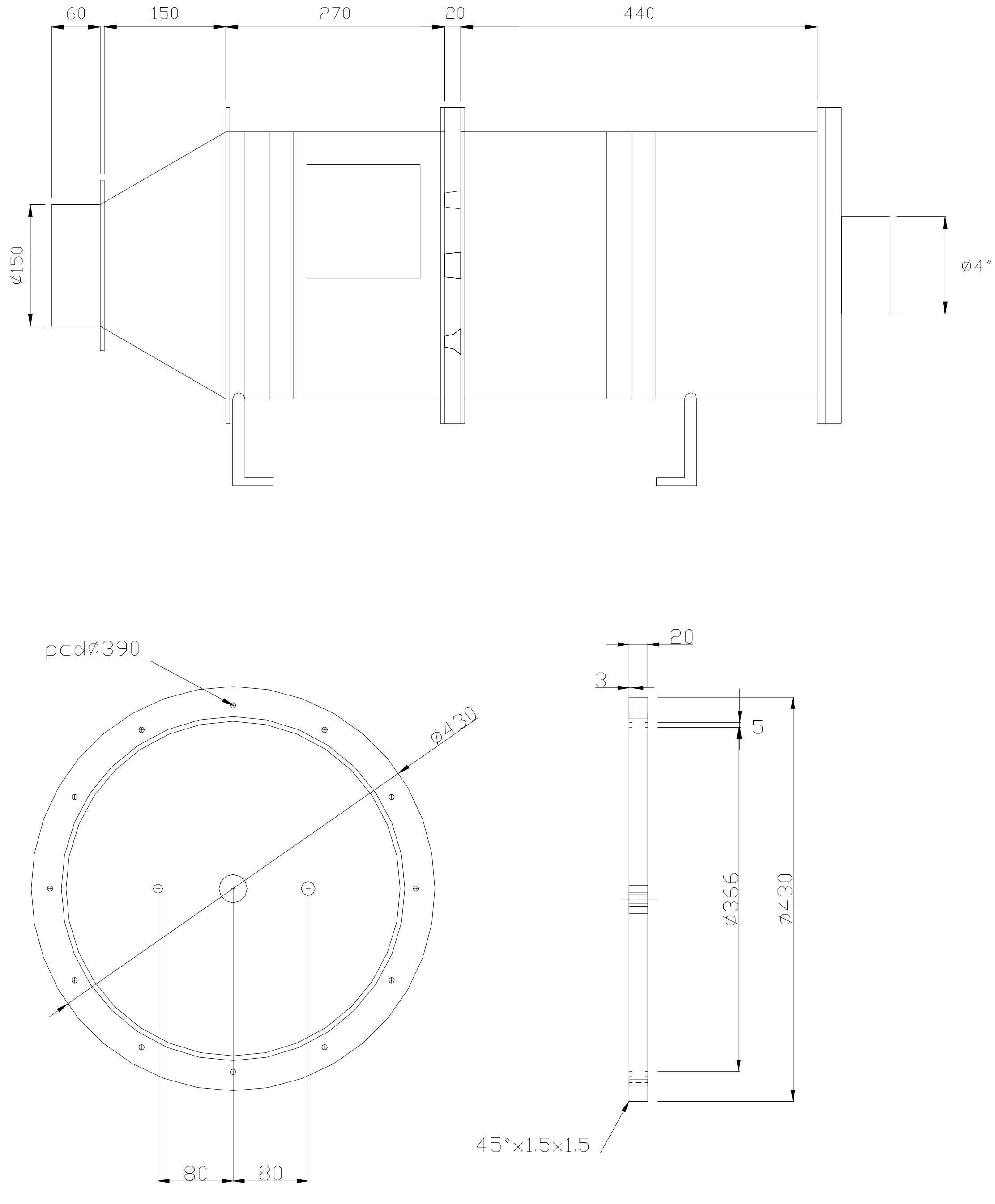

Fig. 2.3 The design of AMCA 210-85 standard

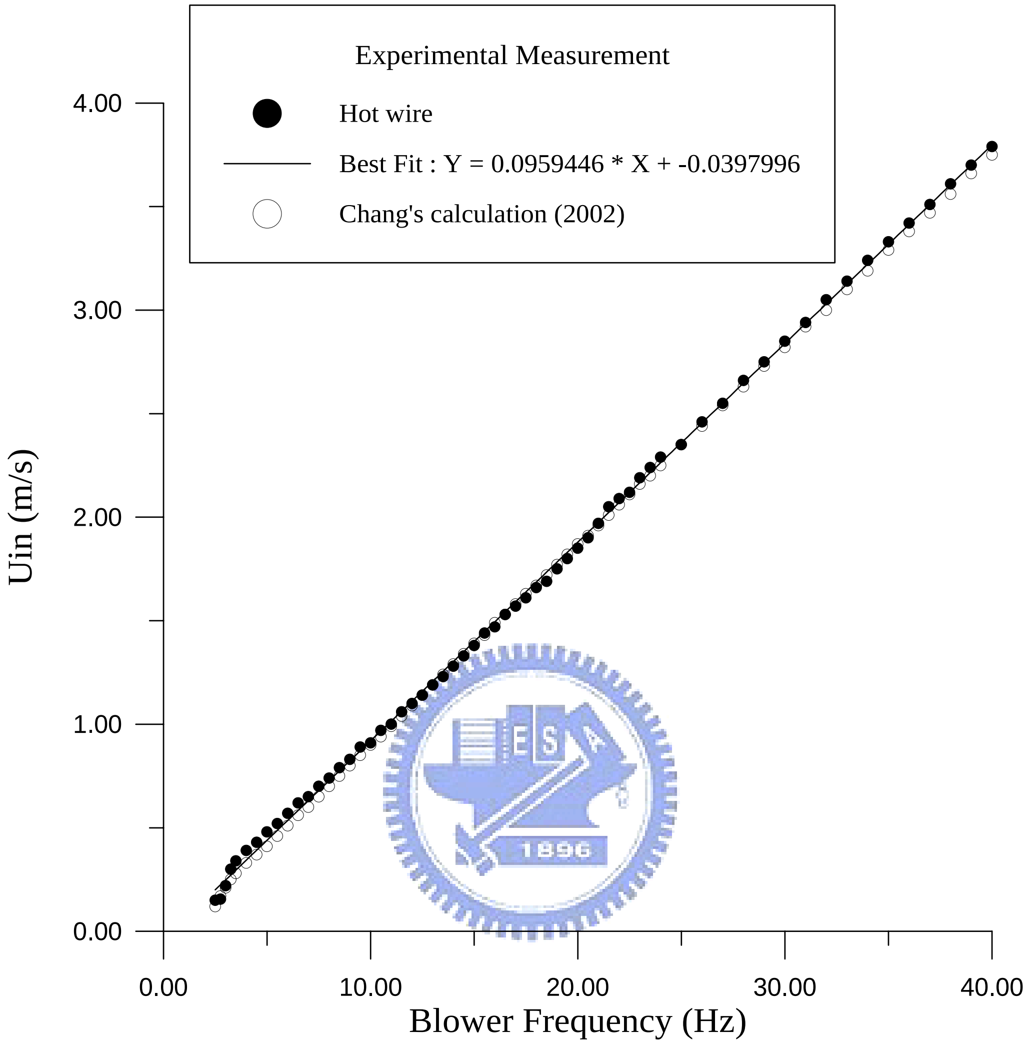

Fig. 2.4 The relation figure of blower frequency and airflow velocity

Fig. 2.5 The bases of wind tunnel and blower are separated by a flexible plastic ductwork

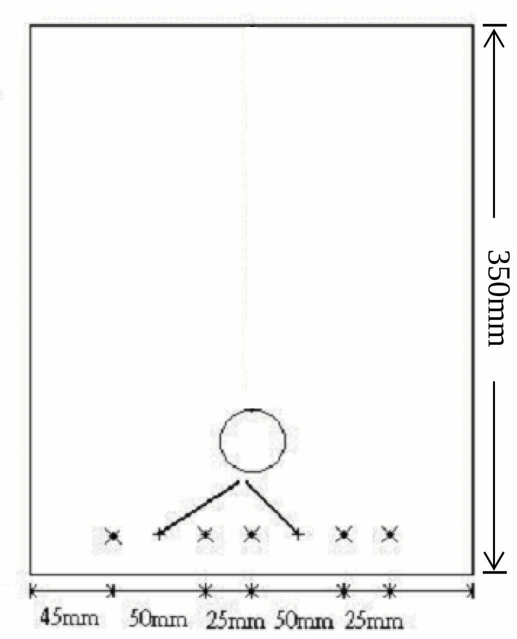

Fig. 2.6 The positions of hot wire sensors

Fig. 2.7 Porous cylindrical burner and cylindrical brass rod

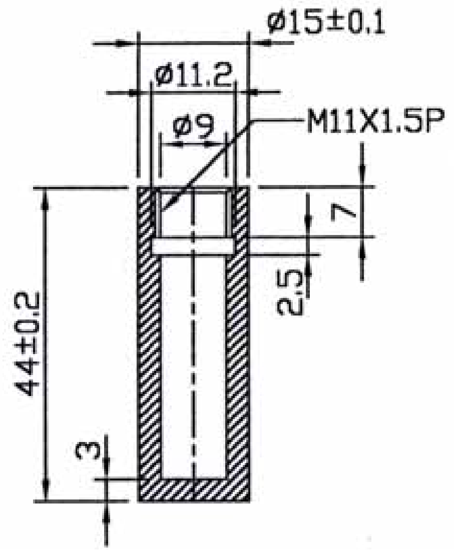

Fig. 2.8 Cylinder of 15mm

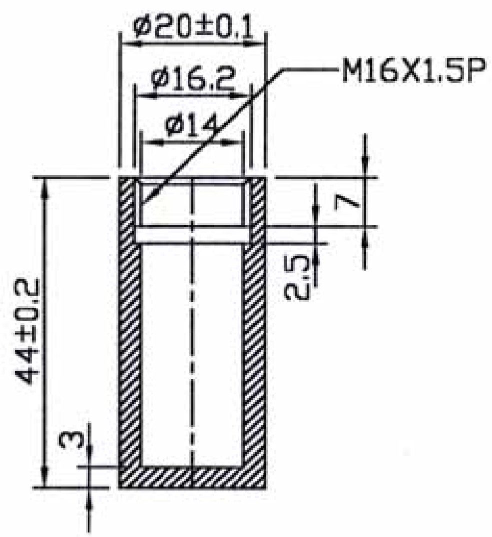

Fig. 2.9 Cylinder of 20mm

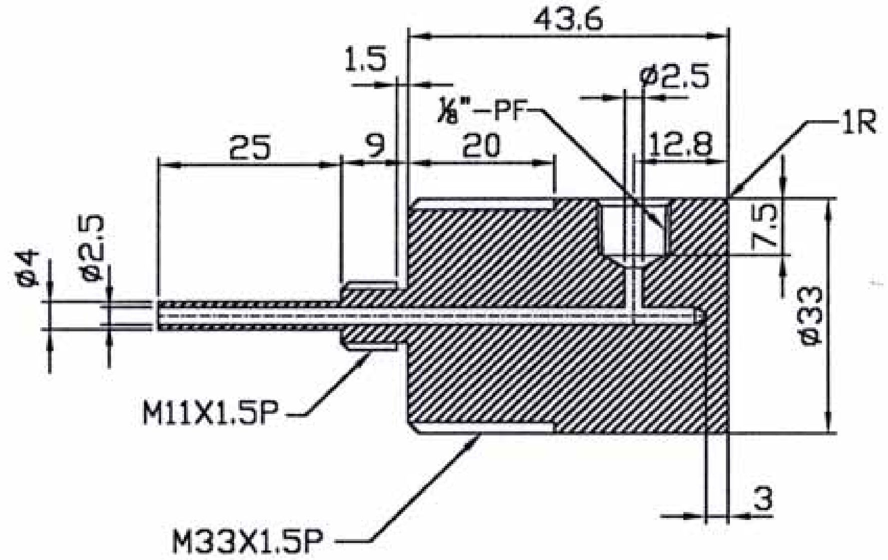

(a)

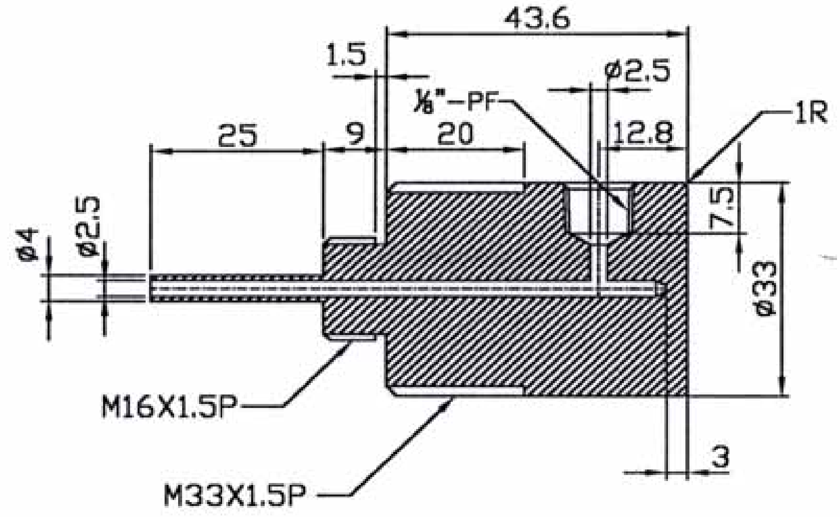

(b)

Fig. 2.10 Cylindrical brass rod for (a) 15mm and (b) 20mm cylinders

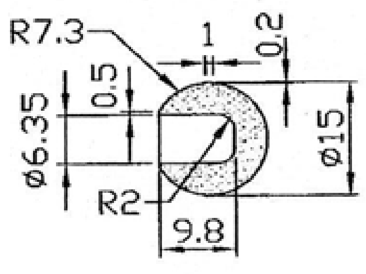

Fig. 2.11 The fillister in porous sphere

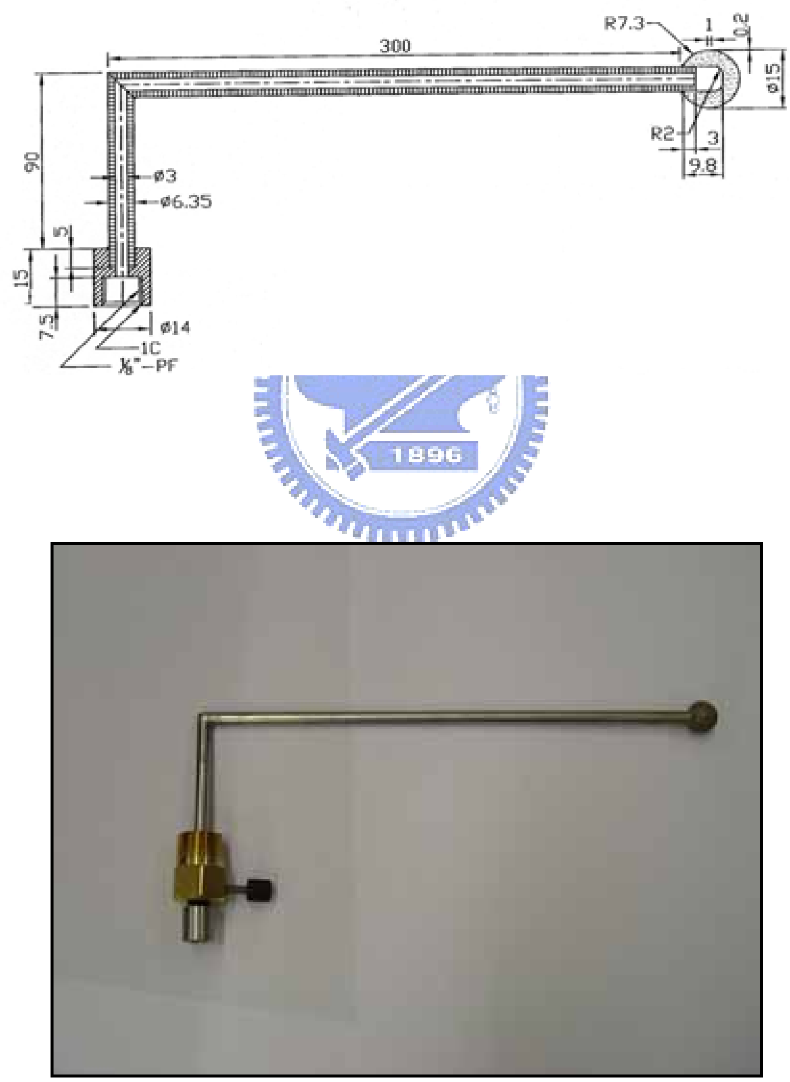

Fig. 2.12 Vertical orientation burner

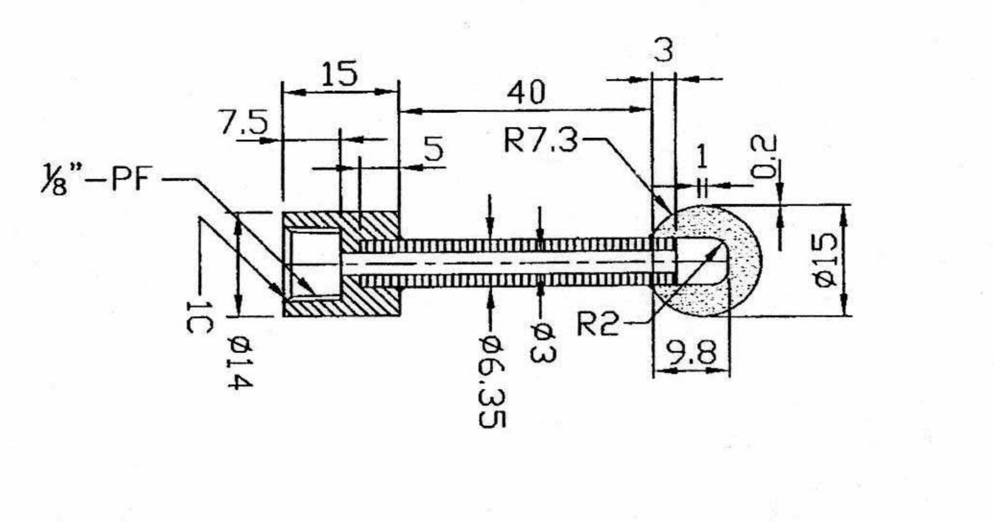

Fig. 2.13 Horizontal orientation burner

Fig. 2.14 Hot wire

Fig. 2.15 IFA 100 Diagnostics

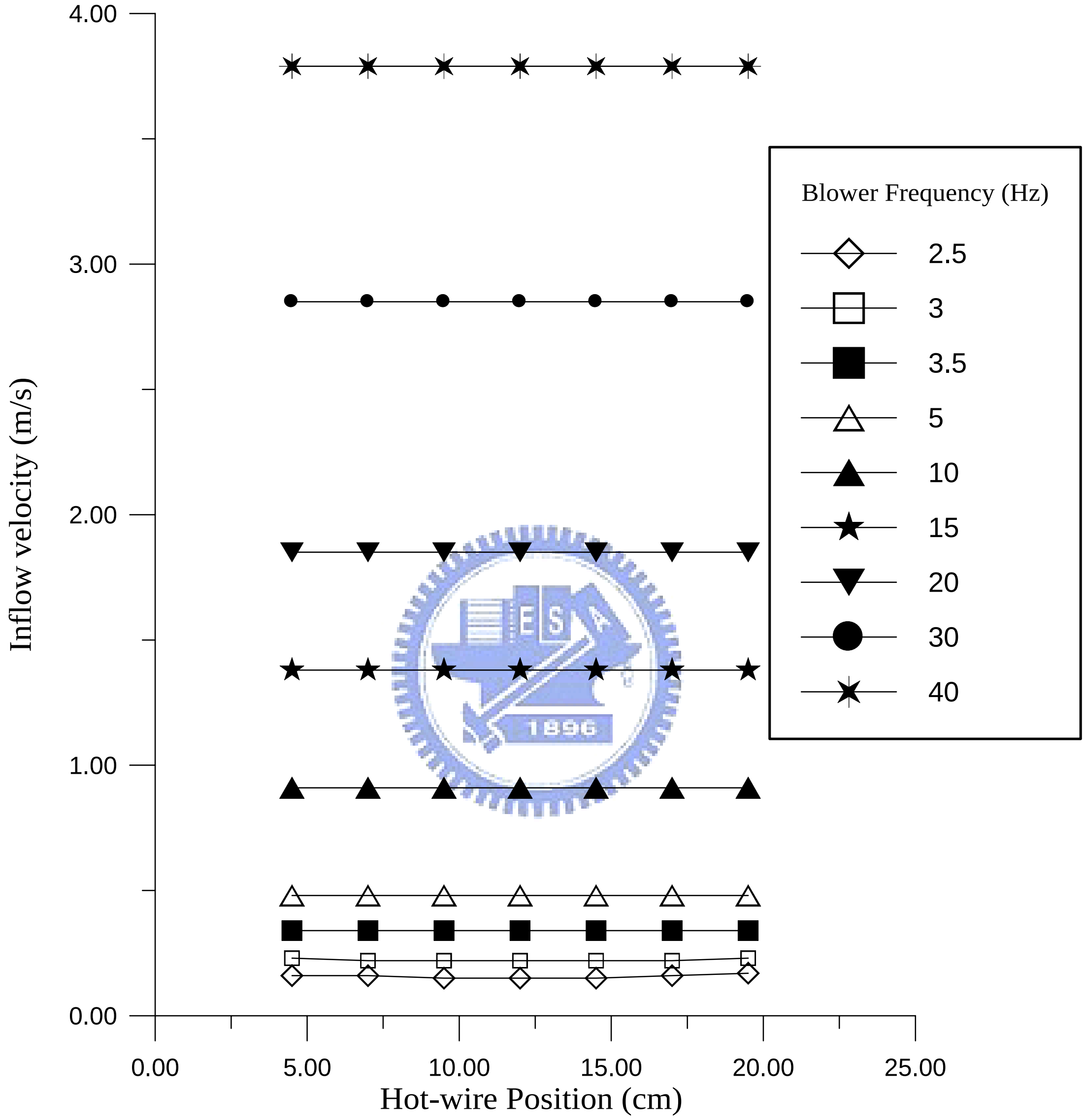

Fig. 2.16 Inflow velocity at each position in the test section

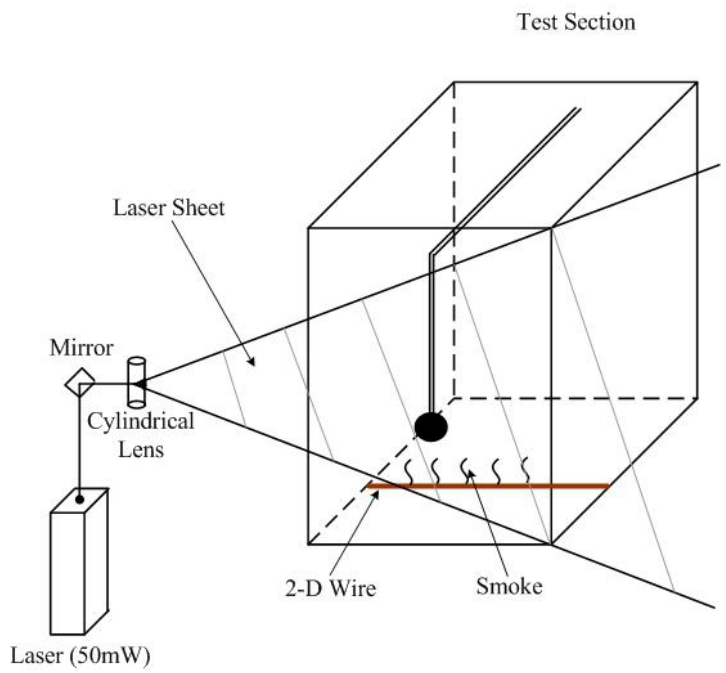

Fig. 2.17 The schematic configuration of smoke wire

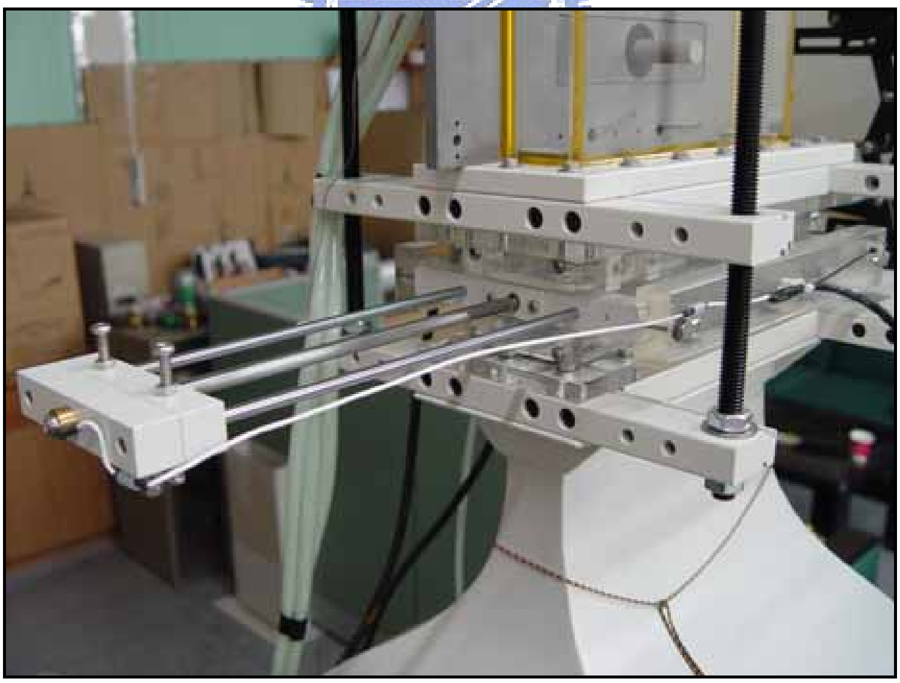

Fig. 2.18 The structural configuration of smoke generation

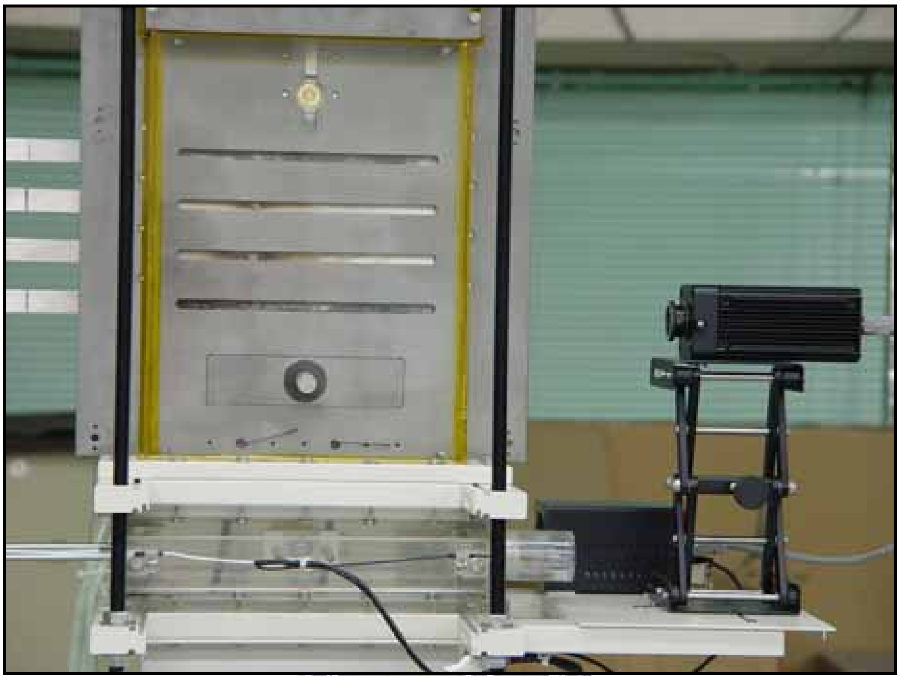

Fig. 2.19 Arrangement of Laser

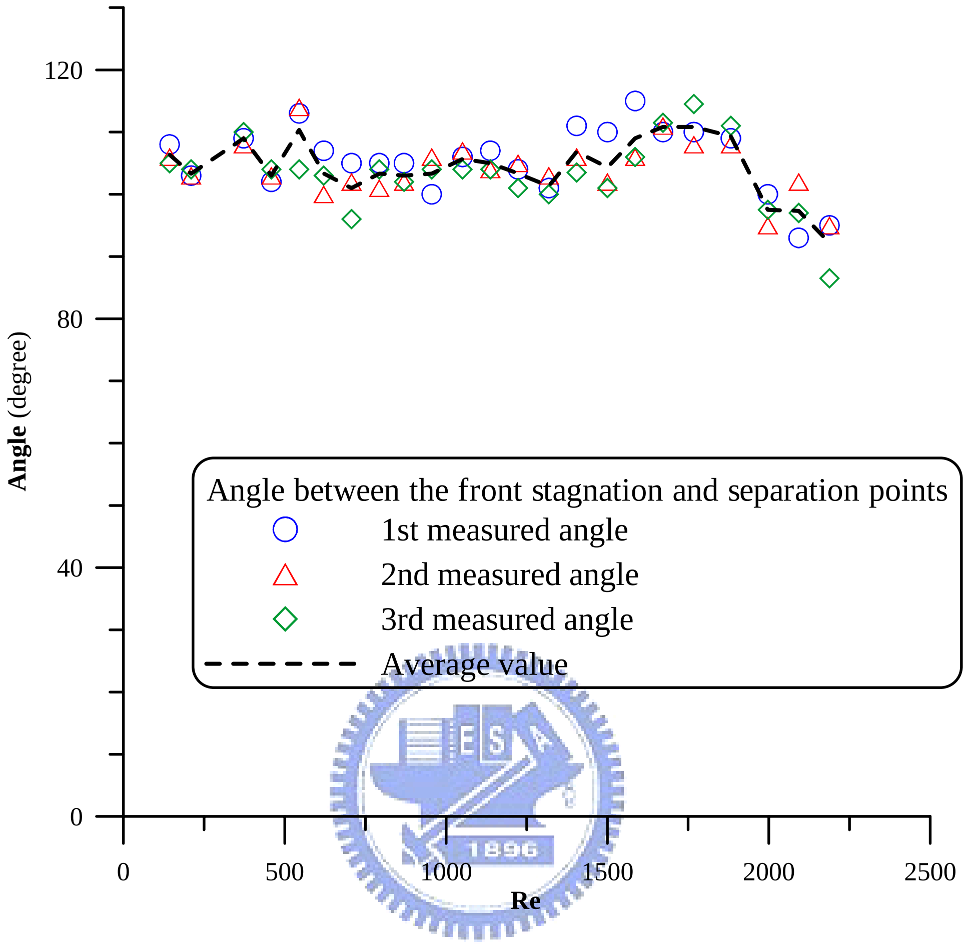

Fig. 3.1 The diagram of experimental repeatability

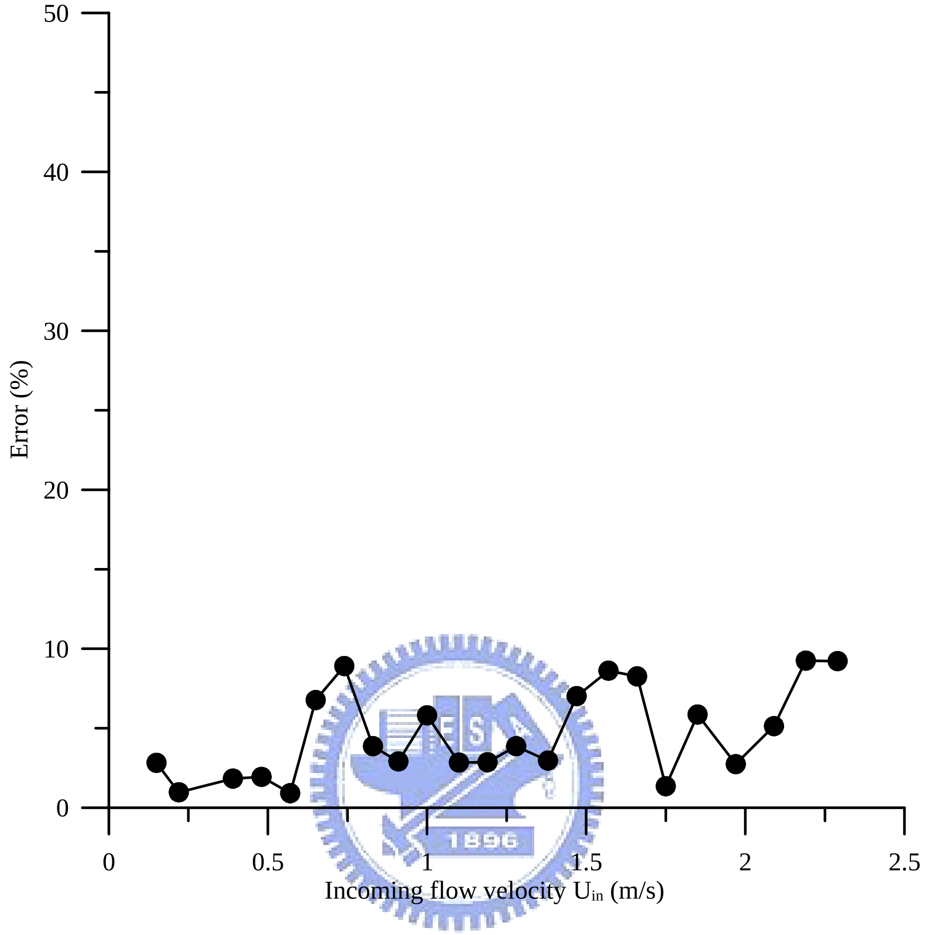

Fig. 3.2 The errors of experimental repeatability

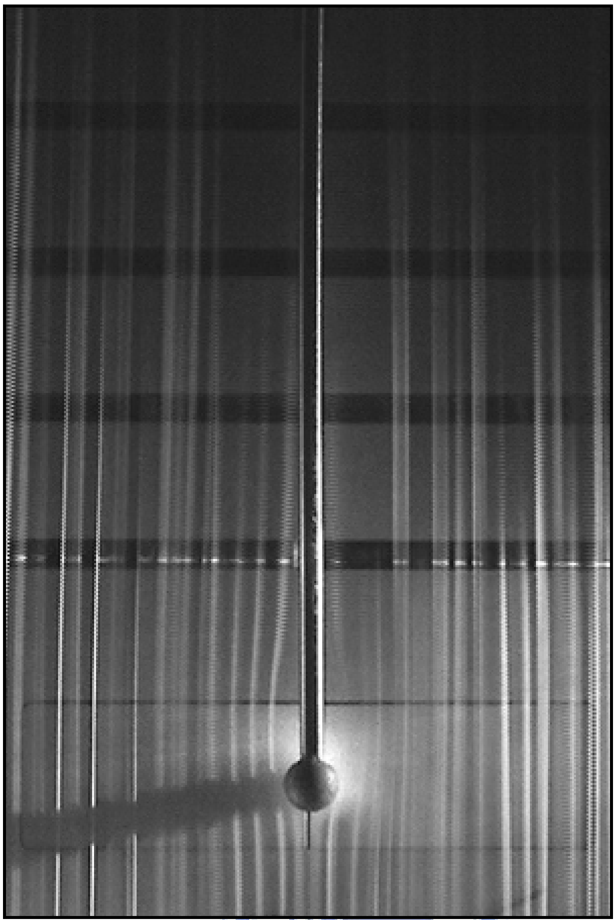

Re = 2,092

Fig. 4.1 Flow past the burner in vertical orientation parallel to the flow stream

(a) Re = 143

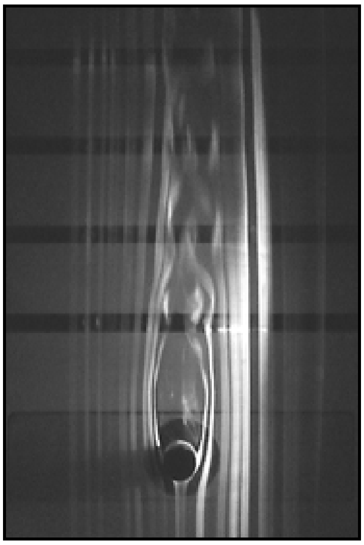

(b) Re = 210

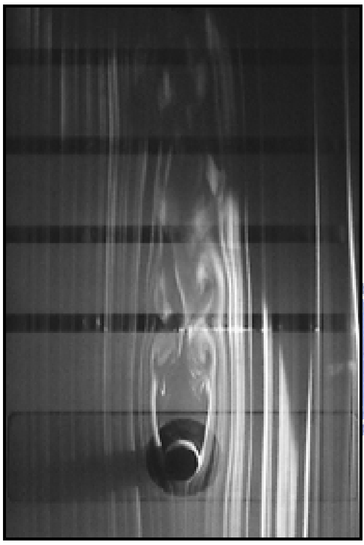

(c) Re = 372

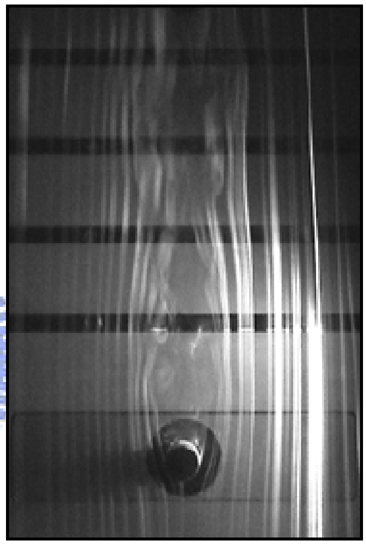

(d) Re = 544

(e) Re = 707

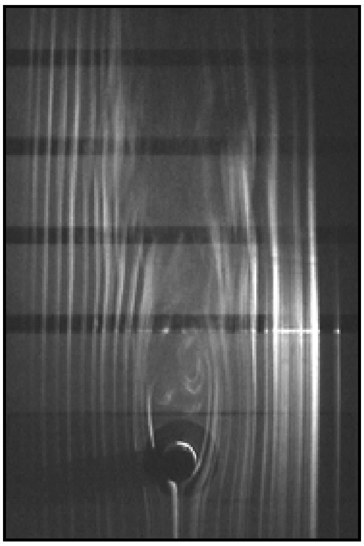

(f) Re = 1,050

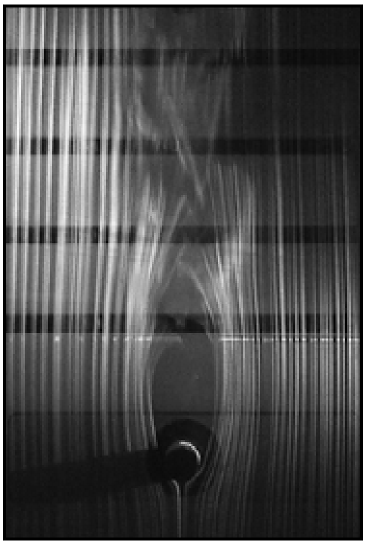

(g) Re = 1,500

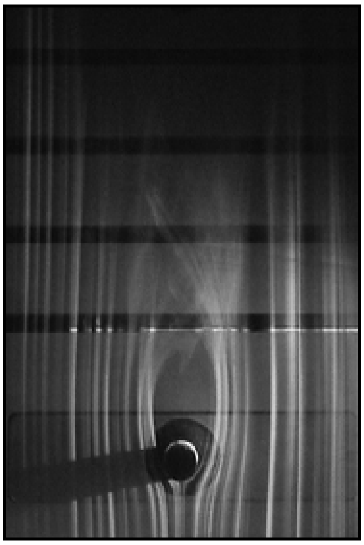

(h) Re = 2,092

Fig. 4.2 Series of flow behaviors as a function of Reynolds number (15mm-diameter cylinder, $V_w = 0$ cm/s)

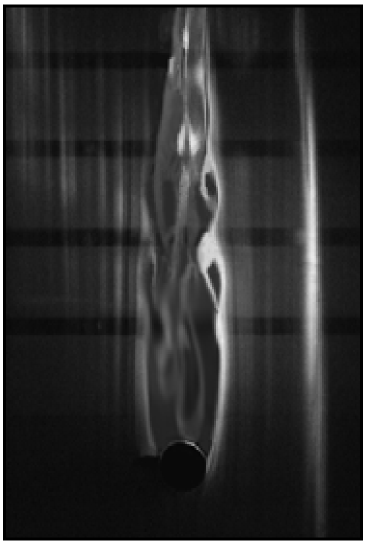

(a) Re = 191

(b) Re = 280

(c) Re = 496

(d) Re = 611

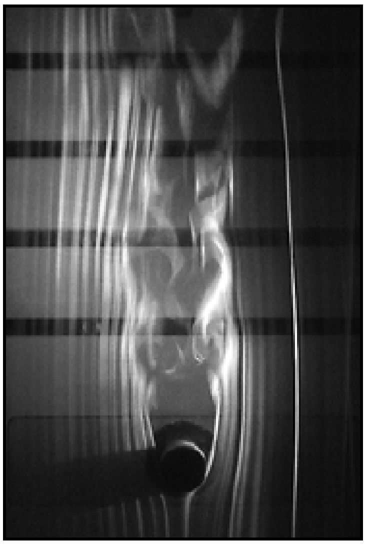

(e) Re = 726

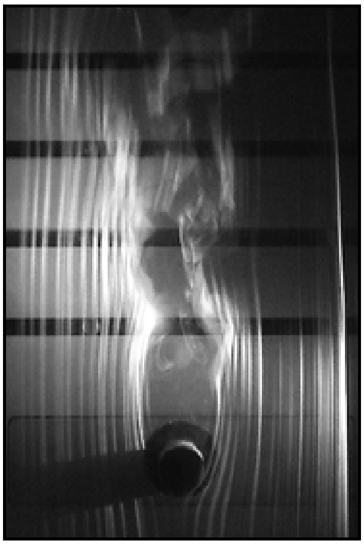

(f) Re = 1,057

(g) Re = 2,000

(h) Re = 2,356

Fig. 4.3 Series of flow behaviors as a function of Reynolds number (20mm-diameter cylinder, $V_w = 0$ cm/s)

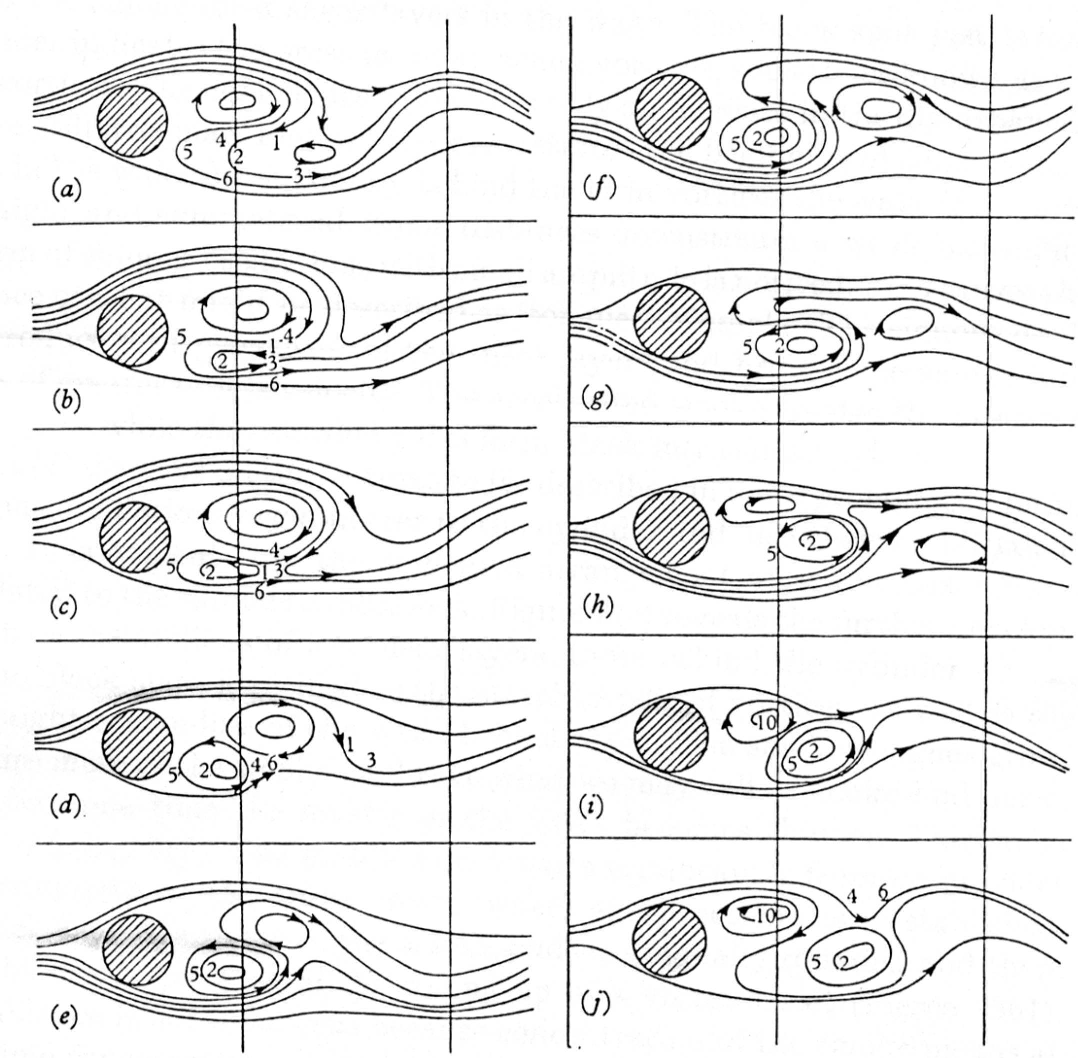

Fig. 4.4 The development of vortices by Nayler and Frazer (1917)

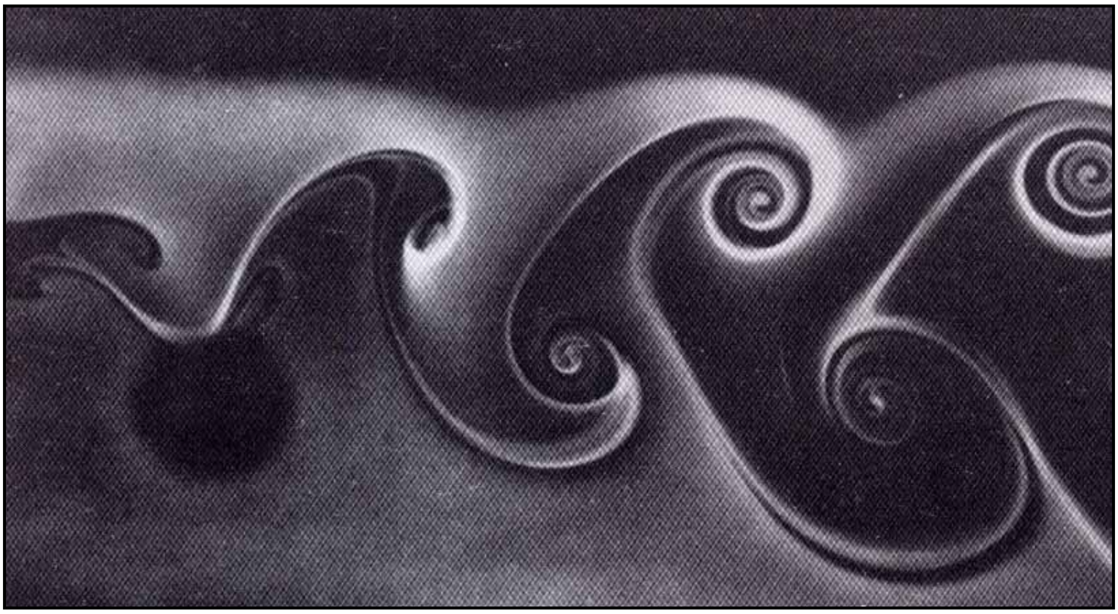

Fig. 4.5 Kármán vortex street behind a circular cylinder at Re = 200.
(Photograph by Gary Koopmann)

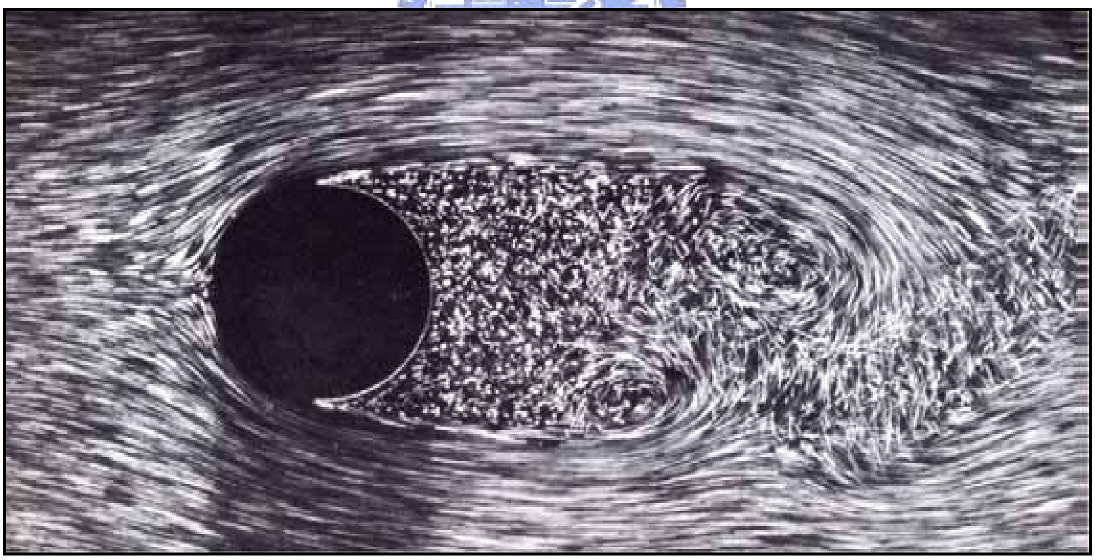

Fig. 4.6 Flow pattern for circular cylinder at Re = 2,000.
(Photograph by Werlé & Gallon 1972)

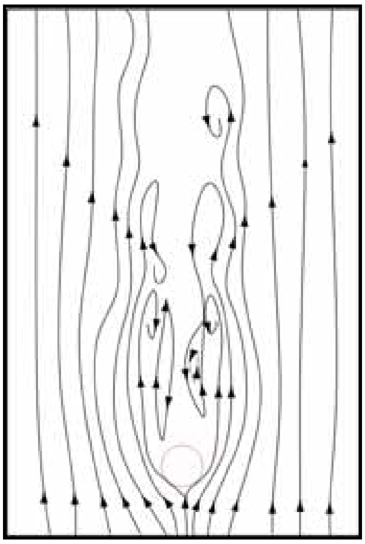

(a) Re =280

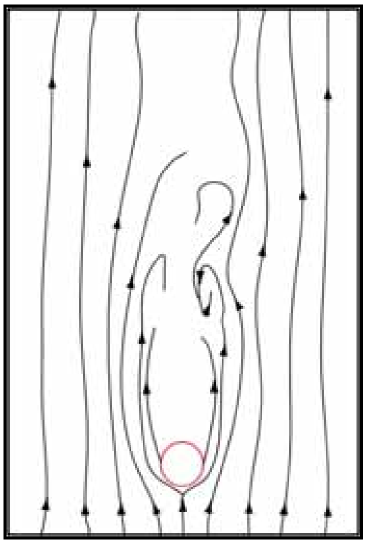

(b) Re = 496

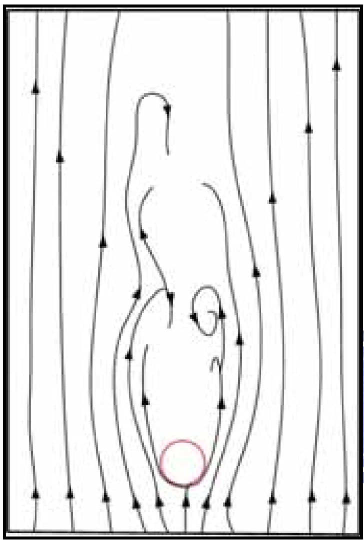

(c) Re = 611

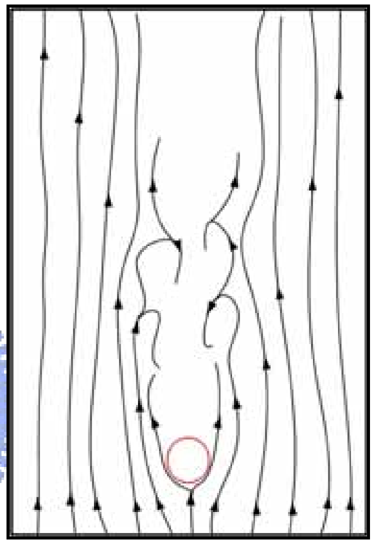

(d) Re = 726

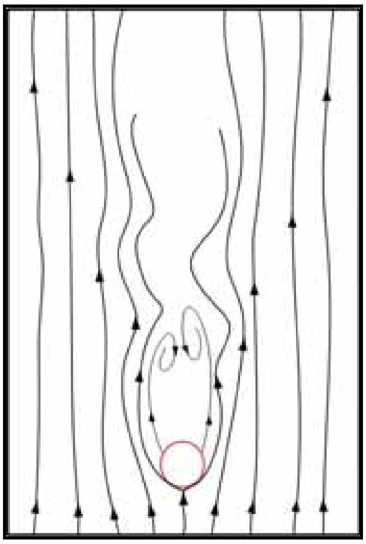

(e) Re 1,057

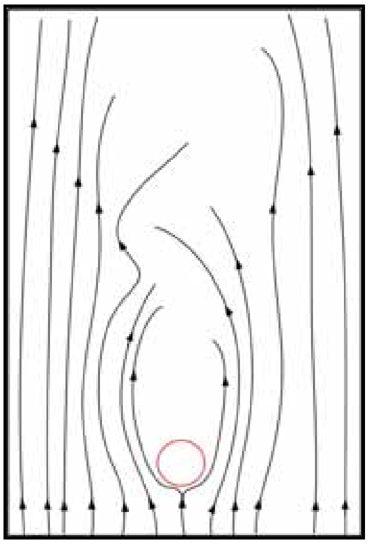

(f) Re = 2,356

Fig. 4.7 Series of schematic sketches corresponded to Fig. 4.3

(a) Re = 143

(b) Re = 210

(c) Re = 372

(d) Re = 458

(e) Re = 621

(f) Re = 1,050

(g) Re = 1,500

(h) Re = 2,092

Fig. 4.8 Series of flow behaviors as a function of Reynolds number (15mm-diameter sphere, V_w = 0 cm/s)

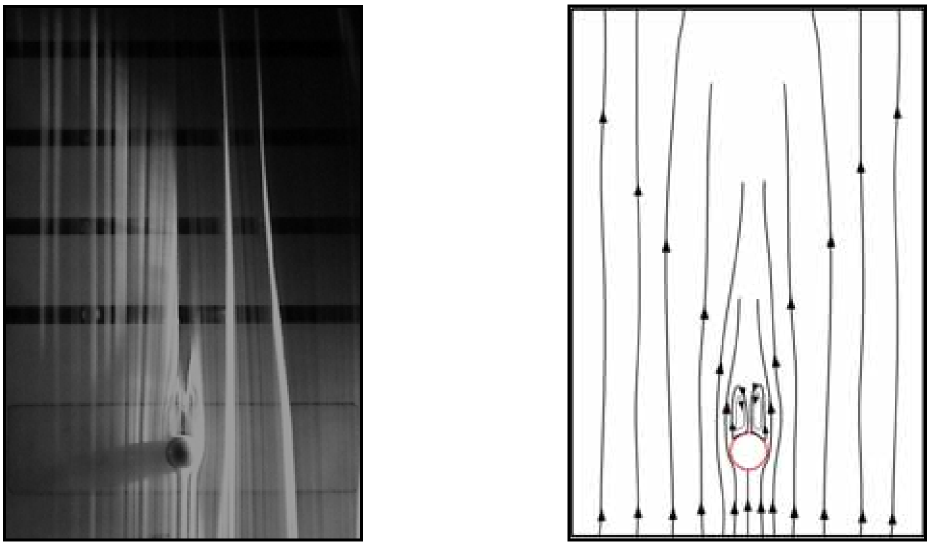

Re = 143

Fig. 4.9 Schematic sketch for 15mm-diameter sphere (V_w = 0 cm/s)

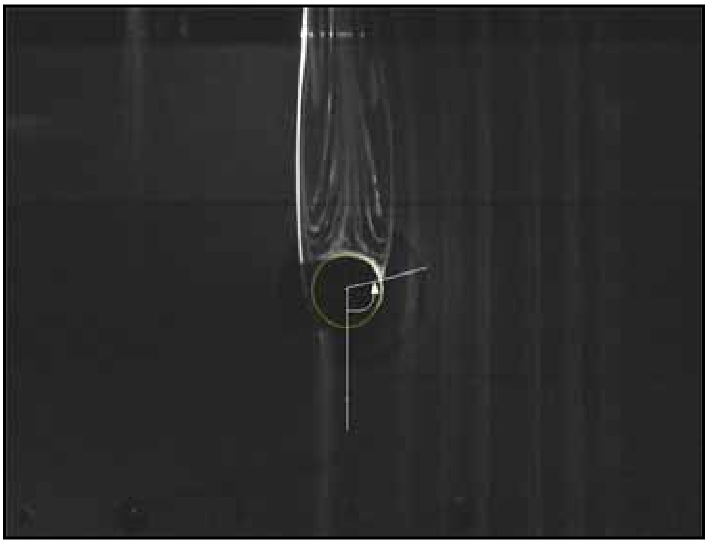

Fig. 4.10 Definition of separation angle θ

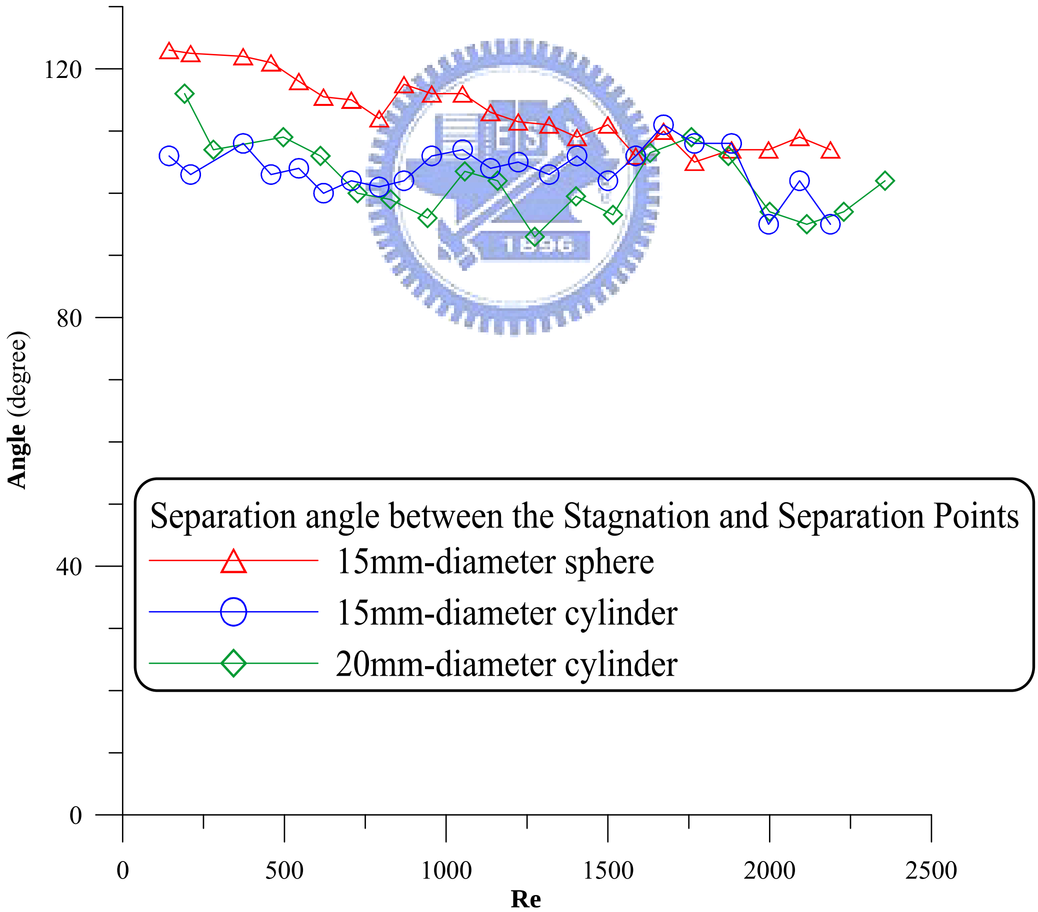

Fig. 4.11 Separation angle θ as function of Re

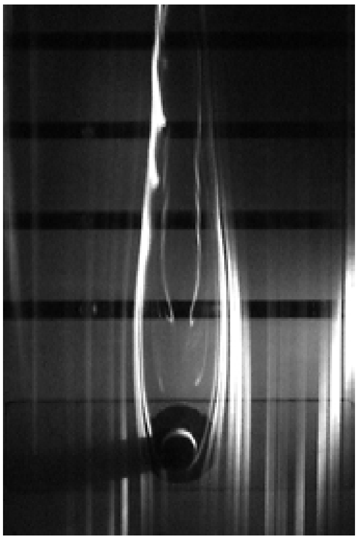

(a) Re = 143

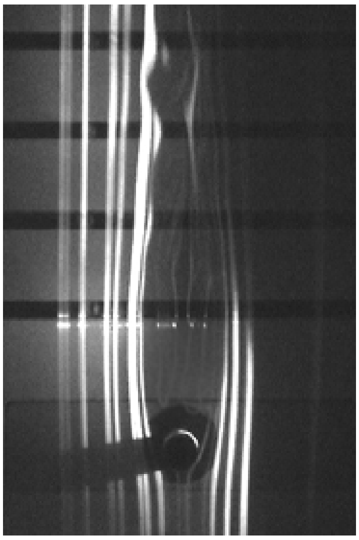

(b) Re = 210

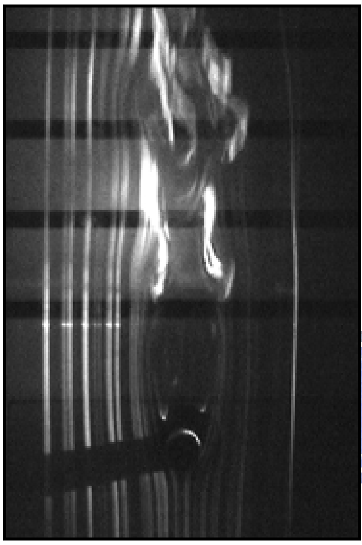

(c) Re = 372

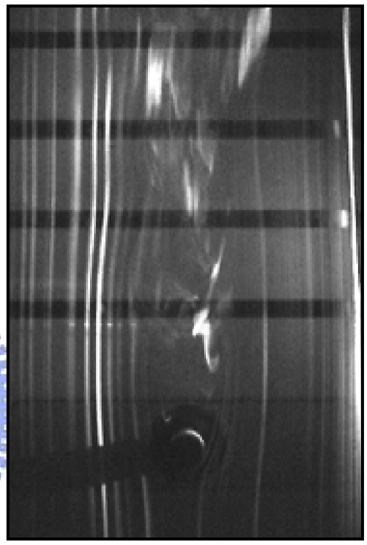

(d) Re = 707

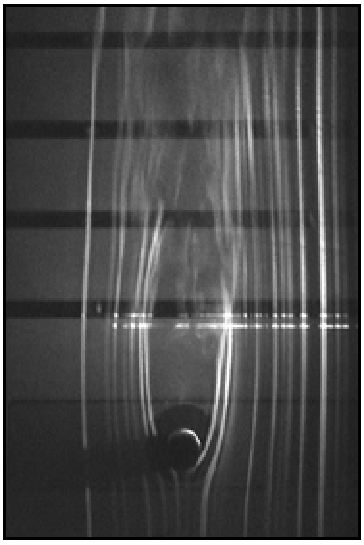

(e) Re = 907

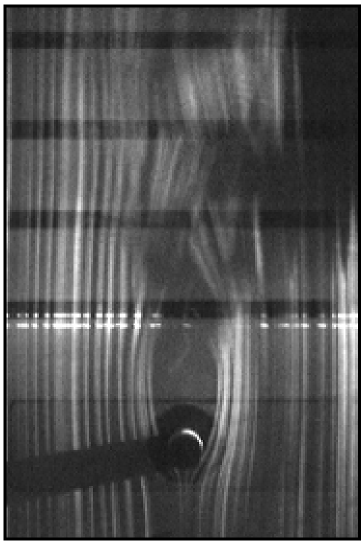

(f) Re = 1,050

Fig. 4.12 Series of flow behaviors as a function of Reynolds number (15mm-diameter cylinder, V_w = 1.76 cm/s)

(a) Re = 191

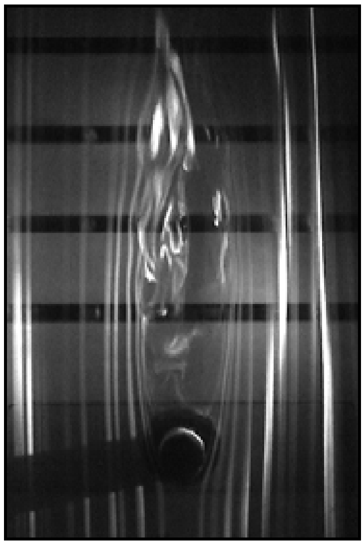

(b) Re = 280

(c) Re = 496

(d) Re= 726

(e) Re = 1,057

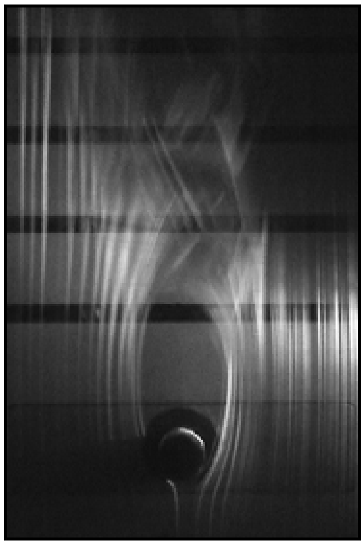

(f) Re = 2,000

Fig. 4.13 Series of flow behaviors as a function of Reynolds number (20mm-diameter cylinder, V_w = 1.32 cm/s)

(a) Re = 143

(b) Re = 210

(c) Re = 372

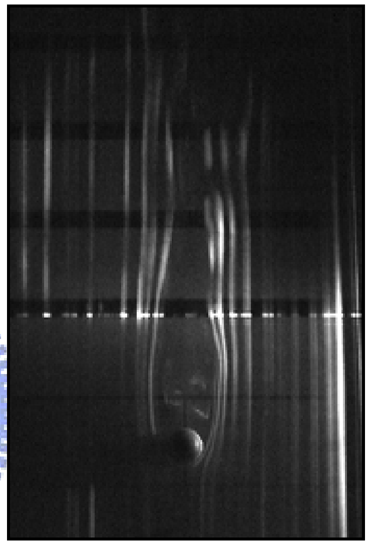

(d) Re = 458

(e) Re = 1,050

(f) Re = 1,720

Fig. 4.14 Series of flow behaviors as a function of Reynolds number (15mm-diameter sphere, V_w = 4.72 cm/s)

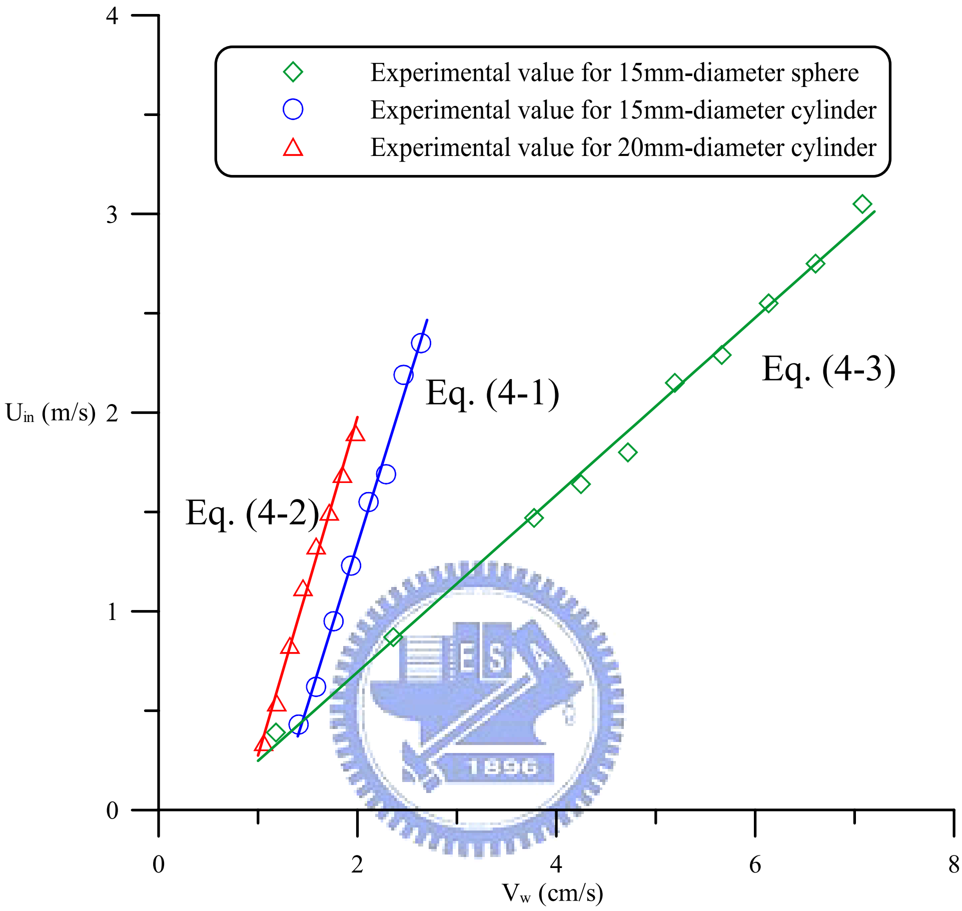

Fig. 4.15 Critical U_{in} as function of V_w

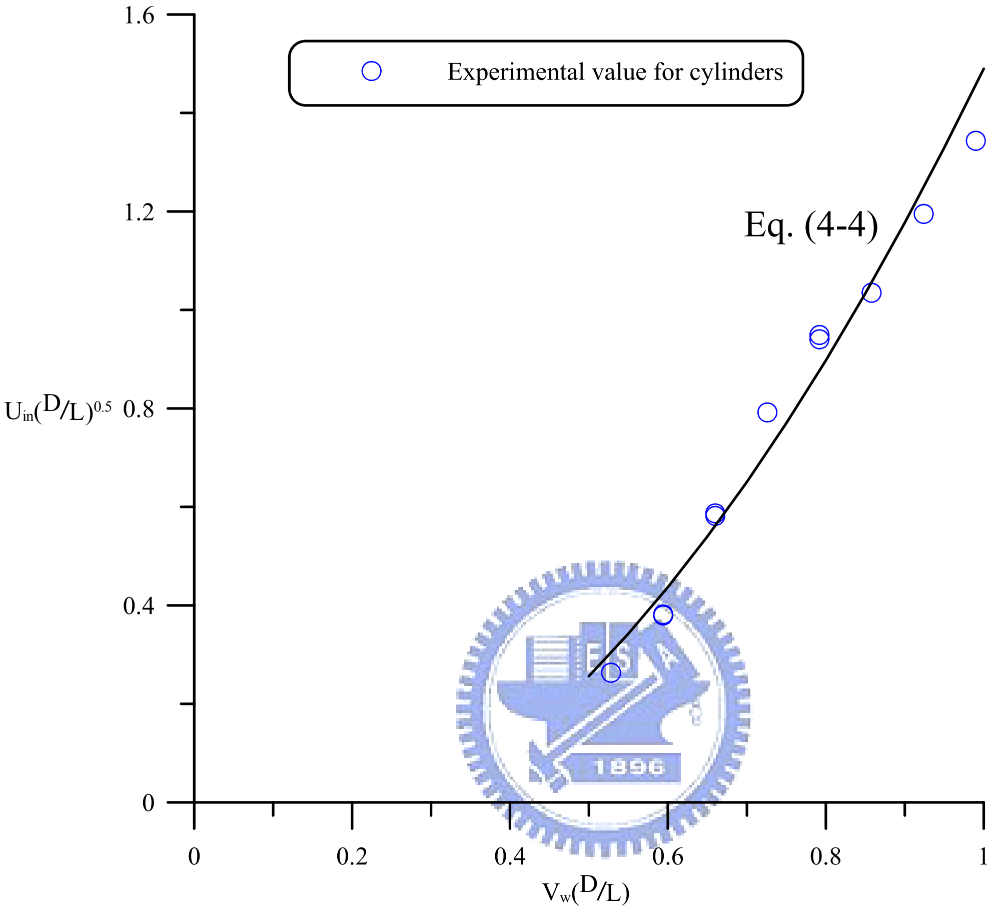

Fig. 4.16 A region map for the wake between blow-off from and return to the rear surface of burner independent of burner's diameter

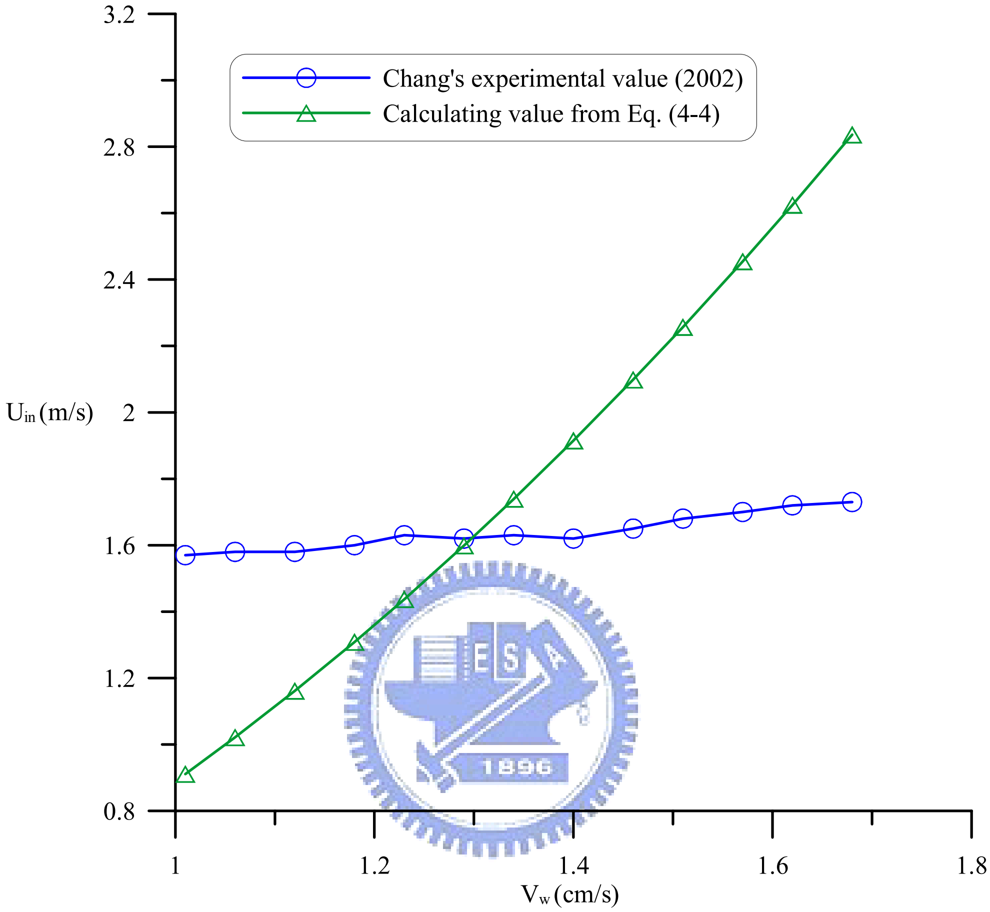

Fig. 4.17 Comparison with Chang's experiment (2002)